Collective behavior based on agent-environment interactions

Gastón Briozzo[1,2,3], Gustavo J. Sibona[1,2], and Fernando Peruani[3]
[1] *Facultad de Matemática, Astronomía, Física y Computación (FaMAFyC), Universidad Nacional de Córdoba (UNC), Ciudad Universitaria (5000), Córdoba, Argentina,*
[2] *Instituto de Física Enrique Gaviola (IFEG), Consejo Nacional de Investigaciones Científicas y Técnicas (CONICET), Ciudad Universitaria (5000), Córdoba, Argentina, and*
[3] *Laboratoire de Physique Théorique et Modélisation (LPTM) (UMR 8089), Cergy Paris Université (CYU), 2 avenue A. Chauvin, Cergy-Pontoise cedex (95302), France*

(Dated: January 16, 2026)

We present a model of active particles interacting through a dynamic, heterogeneous environment, leading to emergent collective behaviors without direct agent-to-agent communication. Expanding the resource-dependent framework introduced in [1], agents perform a persistent random walk combined with chemotaxis, directing toward nutrient-rich patches, whose resources are generated by logistic regrowth. We identify distinct phases of collective organization, ranging from disordered gas-like states to polar traveling waves and nematic independent clusters, depending on the interplay between chemotactic sensitivity and angular noise. The system exhibits spontaneous symmetry breaking and density waves driven purely by the coupling between population dynamics (birth-death processes) and environmental feedback. Our results bridge active matter physics and movement ecology, demonstrating that complex spatiotemporal patterns can arise without direct interaction between agents, but solely from the maximization of resource intake in a reactive environment.

INTRODUCTION

The emergence of collective behavior in systems of self-propelled agents is a widely-observed phenomenon in nature, ranging from bacterial colonies and cell tissues to bird flocks and fish schools [2–4]. Standard models of active matter typically rely on direct interactions, such as alignment forces or steric repulsion, to generate coherent motion [5, 6]. However, in many ecological and biological scenarios, individuals do not necessarily gauge the orientation of their neighbors directly. Instead, they interact through a dynamic environment that serves both as a resource depot and a medium for information transfer [7, 8].

The coupling between agent dynamics and environmental heterogeneity has recently attracted considerable interest, bridging the gap between active matter physics and movement ecology [9, 10]. In a previous work [1], we introduced a framework where active agents consume resources from a logistic environment, storing energy for metabolism and reproduction. That study revealed that survival strategies are dictated by a trade-off between motility and resource availability, leading to distinct static and active phases. However, it treated agent motion as blind to gradients, neglecting the capacity of organisms to sense and react to resource distribution.

In this work, we extend that framework to investigate how indirect interactions mediated solely by the environment can lead to robust collective motion. We introduce chemotaxis into the agent dynamics [11, 12], allowing individuals to bias their persistent random walk toward nutrient-rich areas. Unlike classical chemotactic models where the chemoattractant diffuses fast, here the "field" is the nutrient landscape itself, which is shaped by the history of consumption by the population. We show that this agent-environment feedback loop is sufficient to break the symmetry of the system, giving rise to polar traveling waves, pulsating clusters, and nematic patterns. By analyzing the interplay between alignment sensitivity and angular noise, we study the different phases of the system, demonstrating that direct social forces are not a prerequisite for the emergence of complex order in active populations.

INDIVIDUAL-BASED MODEL (IBM)

An ecological environment consists of a space that contains both nutrients and biological entities that need them to survive. The concentration of these resources is described by the *food field* $f(\mathbf{x}, t)$, discretized into identical square patches that tessellate the space. The time evolution of the available resources in a patch follows a logistic function, with *growth rate* r and *capacity* c, plus a depletion term q due to the agents' *intake rate*. Agents are modeled as disks of *radius* R that interact with each other via a *soft-body potential* U, which penalizes overlapping. They explore space performing a persistent random walk [13, 14] with constant *active velocity* v_0 and changing direction randomly with an *angular diffusion coefficient* D_θ (see [1]). Moreover, agents actively rotate following the *food gradient* ϕ with an *alignment force* γ, performing chemotaxis. While in a patch, agents can take energy from it at intake rate $q = I_c \tanh[I_s f(\mathbf{x}, t)/I_c]$, where I_c is the *intake capacity* and I_s the *intake slope*. These resources are stored in agents' *inner energy de-*

pot e, to be later consumed in metabolic expenditures with *metabolic rate* m or convert it into kinetic energy with *kinetic rate* k [15, 16]. Food is also used for survival and reproduction. Those agents whose inner energy is below the *starvation energy* e_s will die. Meanwhile, those agents whose inner energy is above the *reproduction energy* e_r will reproduce, and both inner energies (agent and offspring) will be restored to a *birth energy* e_b. We consider $e_s < e_b \leq e_r/2$, so that reproduction may have an energy expenditure, but does not kill the agents. Thus, *population size* $N(t)$ and resource distribution $f(\mathbf{x}, t)$ become emergent properties of the system.

The evolution equations for f and the i-th agent are

$$\begin{aligned}
\dot{f}(\mathbf{x},t) &= rf(\mathbf{x},t)\left[1-\frac{f(\mathbf{x},t)}{c}\right] - q[f(\mathbf{x},t)]\rho(\mathbf{x},t),\\
\dot{\mathbf{x}}_i(t) &= v_0\hat{\theta}_i(t) - \nabla U[\mathbf{x}_i(t)],\\
\dot{\theta}_i(t) &= \gamma\sin\left[\phi_i(t)-\theta_i(t)\right] + \sqrt{2D_\theta}\xi_i(t),\\
\dot{e}_i(t) &= q[f(\mathbf{x}_i,t)] - me_i(t) - kv_0^2,
\end{aligned} \tag{1}$$

where $\rho(\mathbf{x}, t)$ is the agents density, the *hat* operator denotes a unit vector $\hat{\alpha} = (\cos\alpha, \sin\alpha)$, and ξ is a Gaussian noise such that $\langle\xi_i(t)\rangle = 0$ and $\langle\xi_i(t_1)\xi_j(t_2)\rangle = \delta_i^j\delta(t_1 - t_2)$. Moreover, $\hat{\phi}_i(t) = \Phi(\mathbf{x}_i, t)/\|\Phi(\mathbf{x}_i, t)\|$ with $\Phi(\mathbf{x}, t) = \int_{\mathbb{R}^2} f(\mathbf{z}+\mathbf{x}, t)\mathbf{z}\kappa(z)d\mathbf{z}$ indicates the "attraction direction" that f generates on the i-th agent (note that it is not exactly a gradient). Here, κ is a short range kernel. Note that agents do not exchange information or interact with each other directly (except for overlapping repulsion), but do so through the environment.

PARTIAL DIFFERENTIAL EQUATIONS (PDE)

Let $\pi(\mathbf{x}, \theta, e, t)$ be the agents *probability density* at position $\mathbf{x}$ with orientation θ and inner energy e at time t. The *regular probability current* will be

$$\mathbf{J}_r = \begin{pmatrix} v_0\cos(\theta) - D_r\partial_x \\ v_0\sin(\theta) - D_r\partial_y \\ \gamma\sin\left[\phi(\mathbf{x},t)-\theta\right] - D_\theta\partial_\theta \\ q\left[f(\mathbf{x},t)\right] - me - kv_0^2 \end{pmatrix}\pi, \tag{2}$$

where D_r is a constant derived from U. But this problem is not regular. Defining $\dot{e}(\mathbf{x}, e, t) = q\left[f(\mathbf{x}, t)\right] - me(t) - kv_0^2$, the *births and deaths probability current* is written as

$$\mathbf{J}_{B\&D} = \begin{matrix} \dot{e}(e_s)\pi(e_s)\Theta[+\dot{e}(e_s)]\Theta(e-e_s) \\ -\dot{e}(e_r)\pi(e_r)\Theta[-\dot{e}(e_r)]\Theta(e-e_r) \\ -2\dot{e}(e_r)\pi(e_r)\Theta[+\dot{e}(e_r)]\Theta(e-e_b) \end{matrix}\begin{pmatrix}0\\0\\0\\1\end{pmatrix}, \tag{3}$$

where Θ is the Heaviside function. So, the total *probability current* is $\mathbf{J} = \mathbf{J}_r + \mathbf{J}_{B\&D}$, and the *Fokker-Planck equation* results

$$\dot{\pi}(\mathbf{x}, \theta, e, t) = -\Box\cdot\mathbf{J}(\mathbf{x}, \theta, e, t) \tag{4}$$

where $\Box = (\partial_x, \partial_y, \partial_\theta, \partial_e)$. All functions, π, $\dot{e}$, $\mathbf{J}$, etc., are assumed to be evaluated at $(\mathbf{x}, \theta, e, t)$ unless explicitly stated otherwise. The $\mathbf{J}_{B\&D}$ current and the boundary conditions $\pi(e) = 0\ \forall e \notin [e_s, e_r]$ guarantee the birth and death processes.

Assuming that θ and e are uncorrelated, we separate $\pi(\theta, e) = \pi_\theta(\theta)\pi_e(e)$, such that $1 = \int_{-\pi}^{\pi}\pi_\theta d\theta$ and $\rho = \int_{e_s}^{e_r}\pi_e de$. We introduce the *n-th polar order moment*

$$\mathbf{P}_n = \begin{pmatrix} P_n^c \\ P_n^s \end{pmatrix} = \int_{-\pi}^{\pi}\int_{e_s}^{e_r}\pi\begin{pmatrix}\cos(n\theta)\\ \sin(n\theta)\end{pmatrix}ded\theta, \tag{5}$$

and define the *n-th polar order matrix* $\mathbb{P}_n^\pm$ and the *births and deaths rate* Λ as

$$\mathbb{P}_n^\pm = \begin{pmatrix} P_n^c & P_n^s \\ \pm P_n^s & \mp P_n^c \end{pmatrix}, \quad \Lambda = -\frac{1}{\rho}\int_{e_s}^{e_r}(0,0,0,\partial_e)\mathbf{J}\pi_e de. \tag{6}$$

Thus, the *hydrodynamic equations* result

$$\begin{aligned}
\dot{\mathbf{P}}_n = &-\frac{v_0}{2}\nabla[\mathbb{P}_{n-1}^- + \mathbb{P}_{n+1}^+] + n\frac{\gamma}{2}\hat{\phi}[\mathbb{P}_{n-1}^- - \mathbb{P}_{n+1}^+]\\
&+ [\Lambda - n^2D_\theta + D_r\nabla^2]\mathbf{P}_n.
\end{aligned} \tag{7}$$

Let's assume that the system is homogeneous in the y direction. As $P_{n+1} \ll P_n$, we can neglect $P_n\ \forall n > 1$. The *partial differential equations* result

$$\begin{aligned}
\dot{f} =& rf\left(1-\frac{f}{c}\right) - I_s f\rho,\\
\dot{\rho} =& -v_0\partial_x P + \left(\Lambda + D_r\partial_x^2\right)\rho,\\
\dot{P} =& -\frac{v_0}{2}\partial_x\rho + \frac{\gamma}{2}\cos\left(\phi-\theta_p\right)\rho\\
&+ \left(\Lambda - D_\theta + D_r\partial_x^2\right)P,\\
\dot{\theta}_p =& \frac{\gamma}{2}\sin\left(\phi-\theta_p\right)\frac{\rho}{P},
\end{aligned} \tag{8}$$

where $P\hat{\theta}_p = \mathbf{P}_1$. Here we are assuming that the system is globally homogeneous in the y direction, but that locally the polarization has an angle θ_p.

NUMERICAL RESULTS

To study the evolution of the model described above, we performed simulations starting from a completely random state. Unless explicitly stated otherwise, we use the set of parameters described in the Appendix .

Collective Behavior

Unlike standard flocking models that rely on direct alignment forces, collective behavior in this system emerges solely from indirect interactions mediated by the resource field. As agents consume resources, they generate dynamic gradients that, coupled with the logistic

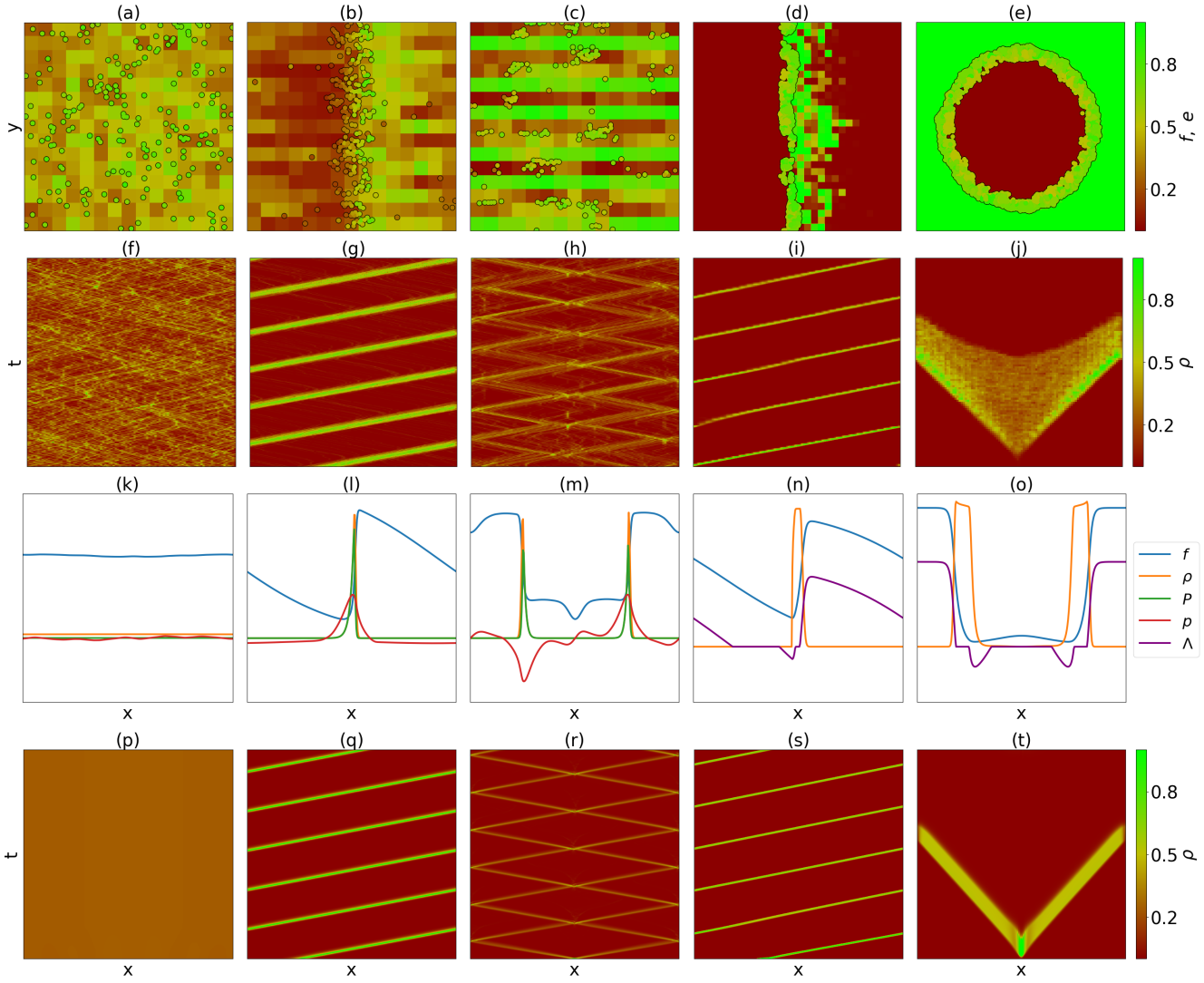

FIG. 1. **Emergent collective phases: Comparison between IBM and PDE.** (**a-j**) Individual-Based Model (IBM) results. (**k-t**) Continuum (PDE) solutions. **Top row** (**a-e**): Snapshots of agent spatial distribution and inner energies. **Second row** (**f-j**): Kymographs showing the time evolution of agent density. **Third row** (**k-o**): Numerical solutions of the fields from Eq. (8). **Bottom row** (**p-t**): PDE density kymographs. The columns correspond to different dynamical regimes driven by the alignment force γ: **Left column** (Gas phase): $v_0 = 0.70$, $D_\theta = 0.01$, $\gamma = 0.01$. For $\gamma < \gamma_p$, angular noise dominates, resulting in a globally homogeneous, disordered state. **Second column** (Polar order): $\gamma = 0.10$. In the regime $\gamma_p < \gamma < \gamma_n$, spontaneous symmetry breaking occurs, leading to periodic traveling waves. **Third column** (Nematic order): $\gamma = 1.00$. For $\gamma > \gamma_n$, the wavefronts fragment into compact, independent clusters with opposing velocities (ripple effect). **Fourth & Right columns** (Proliferation waves): $v_0 = 0.05$, $D_\theta = 0.05$, $\gamma = 0.00$. In the absence of chemotaxis, slow diffusion coupled with birth-death dynamics drives the emergence of planar (fourth column) and circular (right column) density waves. See Supplemental Material for descriptive videos.

recovery of patches, create a feedback loop guiding the population via chemotaxis. The macroscopic state of the system is governed by the interplay between the chemotactic alignment strength γ and the angular diffusion D_θ.

In the noise-dominated regime ($\gamma < 2D_\theta$), the system remains in a disordered gas phase where environmental fluctuations are insufficient to overcome stochastic reorientation (see Fig. 1, left column). Exceeding the threshold $\gamma > 2D_\theta$ triggers a spontaneous symmetry breaking, leading to a polar ordered phase characterized by robust traveling waves (Fig. 1, second column). Here, agents form compact fronts that chase regenerating resources, exhibiting localized back-flow and secondary transverse modes. At higher sensitivities ($\gamma > \gamma_n$), the coherence of the broad wavefronts is lost. The system transitions into a state of intermittent collective dynamics, where the population fractures into high-density, independent clusters (Fig. 1, third column). These groups exhibit nematic

order on a global scale, forming opposing wavefronts that periodically collide and merge in a "ripple effect".

Even in the absence of chemotaxis ($\gamma = 0$), the coupling between rapid proliferation and local depletion is sufficient to drive density waves, solely due to the demographic pressure of birth-death cycles (Fig. 1, fourth and right columns), distinct from the chemotactic waves driven by alignment.

The third and fourth columns on Fig. 1 proves that the hydrodynamic PDE description captures these complex phenomenological regimes with remarkable agreement to the IBM simulations.

System Phases

To characterize the emergent macroscopic states, we analyze the steady-state population density $n_{\text{eq}} = N_{\text{eq}}/M$ alongside three order parameters: the spatial entropy S, the global polarization P, and the nematic order Q. The entropy, defined as $S = (MS_0)^{-1}\sum_j (n_j/N)\ln(n_j/N)$ with normalization S_0, quantifies spatial heterogeneity ($S \approx 1$ corresponds to homogeneity). The orientational order is captured by $P = |N^{-1}\sum_k e^{i\theta_k}|$ and $Q = |N^{-1}\sum_k e^{i2\theta_k}|$, measuring polar alignment and nematic symmetry, respectively.

Fig. 2 maps these observables against the key control parameters: active velocity v_0, chemotactic strength γ, and angular noise D_θ. In the velocity domain (top row), the system exhibits survival only within a finite window $[v_{\min}, v_{\max}]$ defined by metabolic constraints (Eqs. (41) and (42)).

The transition from disorder to order is governed by the competition between alignment and noise (middle and bottom rows). We identify a critical noise-to-alignment ratio $\tau_c = D_\theta/\gamma \approx 0.5$ marking the onset of collective motion. For $\tau > \tau_c$ (noise-dominated), the system is in a disordered gas phase characterized by maximum entropy, vanishing order parameters ($P, Q \approx 0$), and a population density determined solely by local diffusion. For $\tau < \tau_c$ (alignment-dominated), symmetry breaking occurs. The system first enters a polar phase (high P, moderate Q) where traveling waves maximize coherent transport. As γ increases further (or D_θ vanishes), the system transitions into a nematic phase (high Q, decreasing P) where waves fracture into opposing clusters.

Interestingly, the population size n_{eq} is non-monotonic across this transition. It peaks at the edge of disorder ($\tau \approx \tau_c$) before dropping in the ordered regimes. This suggests that while strong order optimizes transport, excessive cohesion ($\gamma \gg D_\theta$) leads to "over-harvesting" efficiency that paradoxically supports fewer individuals than a loosely coordinated swarm. The entropy mirrors this behavior, dropping sharply as the system organizes into compact structures. Thus, the optimal strategy for population maximization lies at the "edge of chaos," balancing sufficient coordination to find resources against enough randomness to prevent local exhaustion.

CONCLUSIONS

We have studied the emergence of collective behavior in a system of active agents interacting via a dynamic resource landscape. By incorporating chemotaxis into the energy-depot model introduced in [1], we demonstrated that environmental feedback acts as an effective alignment mechanism. The depletion of resources by leading agents creates local gradients that steer followers, generating cohesive traveling waves and compact clusters without the need for explicit alignment rules between individuals.

Our results reveal a rich phase diagram controlled by the interplay between chemotactic strength and angular noise. We identified transitions from a disordered gas phase to a polar ordered phase (traveling waves) and, for high sensitivities, to a nematic phase characterized by opposing wavefronts and ripple effects. These transitions are accompanied by spontaneous symmetry breaking. Furthermore, we showed that even in the absence of chemotaxis, density waves can emerge purely from birth-death asymmetry, highlighting the complex coupling between population dynamics and spatial transport.

This work reinforces the concept that the environment is not merely a background for motion but an active participant in the organization of living matter. The "stigmergic" coordination observed here suggests that foraging efficiency and group cohesion in nature may emerge simultaneously from the selfish pursuit of resources.

ACKNOWLEDGMENTS

This work was partially supported by the grants PIP 112- 2015 01- 00644CO and SeCYT-UNC 05/B457. G.B. acknowledges the Beca Interna Doctoral CONICET and the bourses de France Excellence EIFFEL.

AUTHOR CONTRIBUTIONS

The authors contributed to this work as follows:

- **Briozzo G.**: Conceptualization, Methodology, Formal analysis, Software, Investigation, Data curation, Visualization, Writing.
- **Sibona G.**: Conceptualization, Methodology.
- **Peruani F.**: Conceptualization, Methodology.

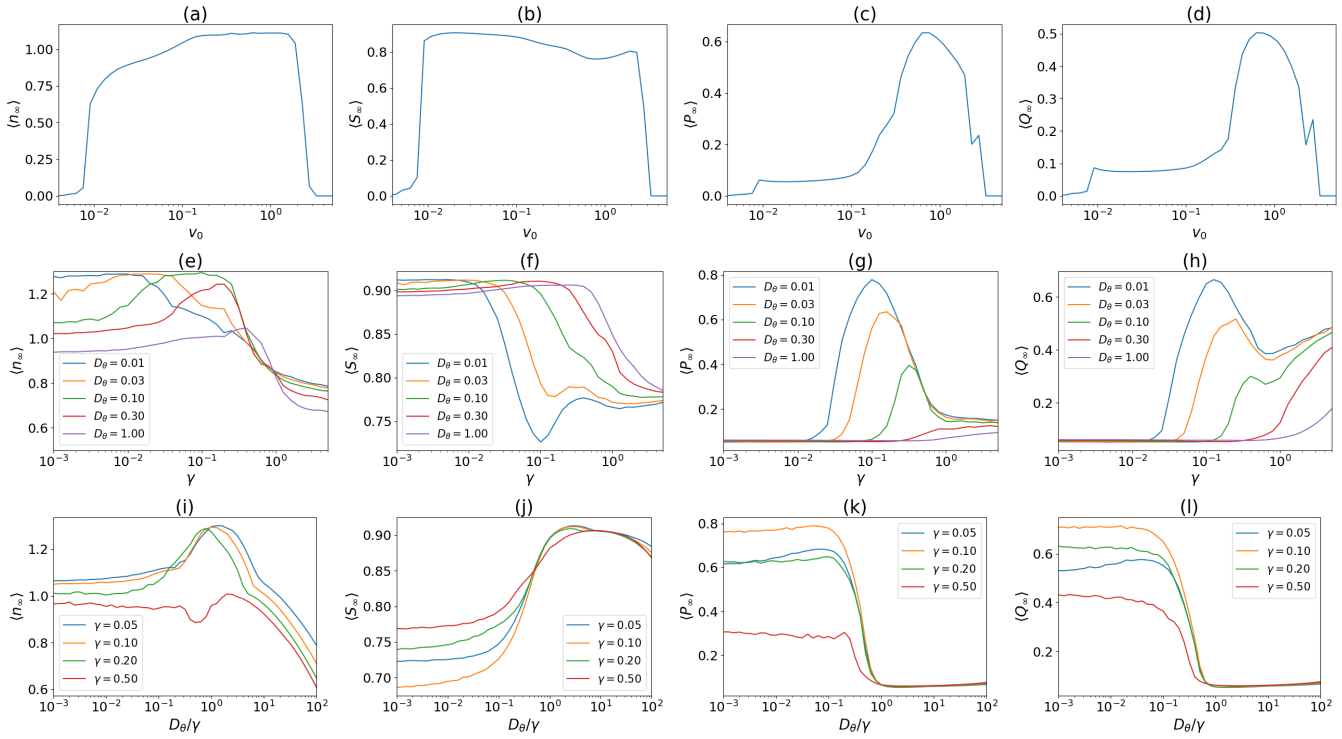

FIG. 2. **Phase diagram and order parameters.** Steady-state averages for population density $\langle n_\infty \rangle$ (1st col), spatial entropy $\langle S_\infty \rangle$ (2nd col), polar order $\langle P_\infty \rangle$ (3rd col), and nematic order $\langle Q_\infty \rangle$ (4th col). **Top row** (**a-d**): Dependence on active velocity v_0. Survival is limited to a window bounded by critical velocities (Eqs. (41), (42)). **Middle row** (**e-h**): Dependence on alignment strength γ. Two transitions are visible: (i) Disorder-to-Polar at $\gamma/D_\theta \approx 2$, where P rises sharply; (ii) Polar-to-Nematic at $\gamma \approx 0.5$, where P declines while Q remains high, indicating wave breakup. **Bottom row** (**i-l**): Dependence on the noise-to-alignment ratio D_θ/γ. The collapse of curves for different γ values highlights D_θ/γ as the primary control parameter for the order transition. Note that population (1st col) peaks near the transition point before decaying in the highly ordered phase, while entropy (2nd col) is minimized in the ordered regimes.

Appendix

Supplementary Material

Drive: `https://drive.google.com/drive/folders/1HPvGuxodZThbz6YHkmhHW2yndGXWdiQF?usp=drive_link`

Parameters

The system will begin with an initial population of $N(0) = M(n_s + n_r)/2$ agents (see Eq. (37)) with radius $R = 1$, metabolic rate $m = 0.005$ and kinetic rate $k = 0.0005$. The environment consists of a square area of size $L = 450$, with periodic boundary conditions, divided into $M = 2025$ square patches of size $L_p = 10$, each of them with a food capacity $c = 1$ and growth rate $r = 0.015$. Agents have an intake slope $I_s = 0.01$ and an intake capacity $I_c = 0.01$. The starvation, reproduction and birth energies are $e_s = 0.1$, $e_r = 0.9$ and $e_b = 0.4$ respectively. These values allow the emergence of stationary populations in equilibrium with the environment. A detailed analysis of them is provided in [1].

Delay Equations

By introducing the *anti-food field* $\psi(\mathbf{x}, t) = 1 - f(\mathbf{x}, t)/c$ and proposing a perturbation around $\psi(\mathbf{x}, t) = 0$ it follows

$$\dot{\psi}(\mathbf{x}, t) = -r\psi(\mathbf{x}, t) + I_c \rho(\mathbf{x}, t), \tag{9}$$

from which are obtained the *delay* equations

$$\begin{aligned} \psi(\mathbf{x}, t) &= I_c \int_0^t e^{-r(t-\zeta)} \rho(\mathbf{x}, \zeta) d\zeta, \\ \Phi(\mathbf{x}, t) &= -\int_0^t e^{-r(t-\zeta)} \int_{\mathbb{R}^2} \rho(\mathbf{z} + \mathbf{x}, \zeta) \mathbf{z} \kappa(z) d\mathbf{z} d\zeta, \end{aligned} \tag{10}$$

which highlights the delayed effect that agents exert on each other via the f field.

Wave Solution

Let's propose a density given by Fourier series

$$\rho = \sum_{m=-\infty}^{\infty} \rho_m e^{i(k_m x - \omega_m t)}. \tag{11}$$

Assuming a constant population $\Lambda = 0$, and solving Eq. (7) for $n = 1$, is obtained that the system forms traveling waves with velocity $\beta_m = v_m/v_0 = (\omega_m/k_m)/v_0$ given by

$$\beta_m = sign(m)\frac{\sqrt{\tau^2+4}-\tau}{2} \tag{12}$$

where $sign(m) = -1$ for $m < 0$ and $sign(m) = +1$ for $m > 0$, and $\tau = D_\theta/\gamma$ is a parameter that indicates the "agents' angular noise" (Fig. 4). The polar order $\mathbf{P} = \mathbf{P}_1$ and the nematic order $\mathbf{Q} = \mathbf{P}_2$ results

$$\begin{aligned} \mathbf{P} &= \sum_{m=-\infty}^{\infty} \rho_m e^{i(k_m x - \omega_m t)} \beta_m \hat{x}, \\ \mathbf{Q} &= \sum_{m=-\infty}^{\infty} \rho_m e^{i(k_m x + \omega_m t)} (2\beta_m^2 - 1)\hat{x}. \end{aligned} \tag{13}$$

If, instead, we solve Eq. (7) for $n = 2$, we get

$$0 = \beta^3 + 2\tau\beta^2 - \beta - \tau, \tag{14}$$

(Fig. 4) and the third order $\mathbf{T} = \mathbf{P}_3$ results

$$\mathbf{T} = \sum_{m=-\infty}^{\infty} \rho_m e^{i(k_m x + \omega_m t)} (4\beta_m^3 - 3\beta_m)\hat{x}. \tag{15}$$

It can be seen that these results are valid only for small values of τ, i.e. $\beta \lesssim 1$. However, this shows that there are stationary solutions in the form of traveling waves.

Fast Angle Approach

Let's consider that the angular dynamics is much faster than the others, so that

$$0 = -\frac{\partial}{\partial\theta}\left[\gamma \sin(\phi - \theta) - D_\theta \frac{\partial}{\partial\theta}\right]\pi, \tag{16}$$

which leads to

$$\begin{aligned} \pi &= \frac{\pi_0}{2\pi} e^{\hat{\phi}\cdot\hat{\theta}/\tau}, \\ \rho &= \pi_0 I_0\left(\tau^{-1}\right), \\ \mathbf{P}_n &= \pi_0 I_n\left(\tau^{-1}\right)\hat{\phi}, \end{aligned} \tag{17}$$

where the π in the denominator is in fact the number pi, not the probability density. Here, I_n is the modified Bessel function of order n. Note that the direction of $\mathbf{P}_n$ is given by the gradient of the food field, $\nabla f/ \mid \nabla f \mid \approx \hat{\phi}$ while its magnitude is directly proportional to ρ and decreases with τ.

However, the real agents density is not instantaneously aligned with the food gradient, but has a direction given by $\hat{p} \approx \hat{\phi}$. We approximate

$$\begin{aligned} g &= g_0 e^{\hat{p}\cdot\hat{\theta}/\tau}, \\ \mathbf{P}_n &= P_n \hat{p}, \end{aligned} \tag{18}$$

where P_n may be a function of time. The evolution equation for the polar order is

$$\dot{\mathbf{P}} = -\frac{v_0}{2}\nabla[\mathbb{I}^-\mathbb{D} + \mathbb{Q}] + \frac{\gamma}{2}\hat{\phi}[\mathbb{I}^-\mathbb{D} - \mathbb{Q}] - D_\theta \mathbf{P}, \tag{19}$$

being $\mathbb{D} = (\rho, 0)$, from where it can be found

$$\begin{aligned} \dot{P} &= \frac{\gamma}{2}\rho\cos(\phi - p) - D_\theta P, \\ \dot{p} &= \frac{\gamma}{2}\frac{\rho}{P}\sin(\phi - p), \end{aligned} \tag{20}$$

by assuming that the angular contribution is much larger than the spatial one and that the nematic order is much smaller than the polar. Assuming that the relaxation time of the polar order magnitude is very short, follows

$$\mathbf{P} = \frac{\tau_c}{\tau}\rho\hat{p}, \tag{21}$$

which is the first order Taylor expansion of Eq. (17).

Analytical Approach

Let us return to Eq. (8) and assume that the four functions of (t, x) are in fact functions of $z = t - x/v_w$. Taking $\hat{p} \sim \nabla f$, the system reduces to

$$\begin{aligned} \dot{f} &= rf\left(1 - \frac{f}{c}\right) - I_s f\rho, \\ \dot{\rho} &= \left(\frac{\gamma}{2}\frac{v_0}{v_w}f_x - D_\theta\right)\rho + D_\theta\rho_0, \end{aligned} \tag{22}$$

where $f_x = -\tanh\left(\dot{f}/N_f\right)$, being N_f a constant. We approximate the term $\nabla f/ \mid \nabla f \mid \cdot\hat{p}$ in Eq. (8) by the term f_x in Eq. (22) since, being in one spatial dimension, the dot product yields only ± 1. Instead, if ∇f is small the agents in a two-dimensional space should disperse, so we take the attraction generated by ∇f to be proportional to it. Eq. (22) admits periodically stable solutions in the form of traveling waves, as shown in Fig. 3 **(a)**.

From Eq. (1) and Eq. (7) up to order $n = 1$, considering $\mathbf{P}_n = 0\ \forall n \geq 2$ and $P_n^s = 0\ \forall n$ it is obtained

$$\begin{aligned} \dot{f} &= rf\left(1 - \frac{f}{c}\right) - I_s f\rho, \\ \dot{\rho} &= -v_0\partial_x P, \\ \dot{P} &= -\frac{v_0}{2}\partial_x\rho + \frac{\gamma}{2}\cos\phi\rho - D_\theta P. \end{aligned} \tag{23}$$

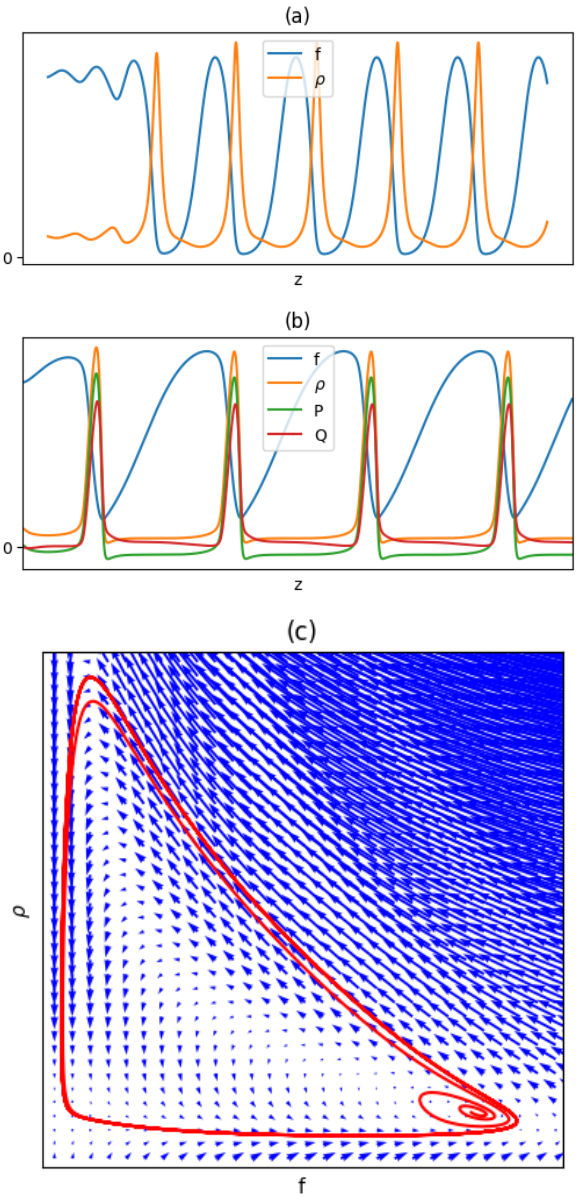

FIG. 3. **(a)**: Numerical integration of Eqs. (22) and (24). **(b)**: Numerical integration of Eq. (26). **(c)**: Phase portrait and orbit from Eq. (24).

Making the change of variable $z = t - x/v_w$, being v_w the wave velocity, and considering $\rho = P/\beta + \rho_0$, the system is reduced to

$$\begin{aligned} \dot{f} &= rf\left(1 - \frac{f}{c}\right) - I_s L_p^2 f\rho, \\ \dot{\rho} &= \left[\left(\frac{\gamma}{2\beta}\cos\phi - D_\theta\right)\rho + D_\theta\rho_0\right]\nu_1, \end{aligned} \tag{24}$$

where $\nu_1 = 2\beta^2/(2\beta^2 - 1)$. Eq. (24) is identical to Eq. (22) except for a proportionality factor ν_1. Thus, Eq. (24) admits stationary solutions in the form of traveling waves, as can be seen in Fig. 3 **(a)** and **(c)**.

Considering now Eq. (7) up to order $n = 2$, it follows

$$\begin{aligned} \dot{f} &= rf\left(1 - \frac{f}{c}\right) - I_s L_p^2 f\rho, \\ \dot{\rho} &= -v_0\partial_x P, \\ \dot{P} &= -\frac{v_0}{2}\partial_x(\rho + Q) + \frac{\gamma}{2}\cos\phi(\rho - Q) - D_\theta P, \\ \dot{Q} &= -\frac{v_0}{2}\partial_x P + \gamma\cos\phi P - 4D_\theta Q, \end{aligned} \tag{25}$$

which, taking $z = t - x/v_w$and $\rho = P/\beta + \rho_0$, reduces to

$$\begin{aligned} \dot{f} &= (r - I_s\rho_0)\, f - \frac{r}{c}f^2 - \frac{I_s}{\beta}fP, \\ \dot{P} &= \left[\beta\gamma\rho_0 f_x - 2\left(\beta D_\theta - \gamma f_x\right)P - (4D_\theta + \beta\gamma f_x)Q\right]\nu_2, \\ \dot{Q} &= \left[\frac{\gamma}{2}\rho_0 f_x - \left(D_\theta - \left(2\beta - \frac{1}{2\beta}\right)\gamma f_x\right)P - \left(4\left(2\beta - \frac{1}{\beta}\right)D_\theta + \frac{\gamma}{2}f_x\right)Q\right]\nu_2, \end{aligned} \tag{26}$$

where $\nu_2 = 2\beta/(4\beta^2 - 3)$. This system of equations also admits stationary solutions in the form of traveling waves, as can be seen in Fig. 3 **(b)**. To linear order, results

$$\partial_t \begin{pmatrix} f \\ P \\ Q \end{pmatrix} = \begin{pmatrix} r - I_s\rho_0 & 0 & 0 \\ \beta\nu_2\gamma D_0(I_s\rho_0 - r) & -2\beta\nu_2 D_\theta & -4\nu_2 D_\theta \\ \nu_2\frac{\gamma}{2}D_0(I_s\rho_0 - r) & -\nu_2 D_\theta & -4\left(2\beta - \frac{1}{\beta}\right)\nu_2 D_\theta \end{pmatrix} \begin{pmatrix} f \\ P \\ Q \end{pmatrix} \tag{27}$$

whose trace and determinant are

$$\begin{aligned} Tr &= (r - I_s\rho_0) - 2(\nu_2 D_\theta)\left(5\beta - \frac{2}{\beta}\right), \\ Det &= 8(r - I_s\rho_0)(\nu_2 D_\theta)^2(2\beta^2 - 1). \end{aligned} \tag{28}$$

Proliferation

Consider a system where food density is given by

$$f(\mathbf{x}, t) = \langle f \rangle + \frac{\sqrt{2D_f}}{I_s}\eta(\mathbf{x}, t), \tag{29}$$

being $\eta(\mathbf{x}, t)$ a Gaussian random variable, so that the energy of the agents satisfies

$$\dot{e}_i = I_s\langle f \rangle - me_i + \sqrt{2D}\eta_i(t). \tag{30}$$

Solving by Sturm-Liouville and keeping the dominant eigenfunction, it can be found

$$\Lambda(\mathbf{x}, t) \approx m\frac{e(\mathbf{x}, t) - e_+}{e_-}, \tag{31}$$

where $e_\pm = (e_r \pm e_s)/2$.

The temporal evolution of the population is given by

$$\dot{N}(t) = \int_{\mathbf{x}} \Lambda(\mathbf{x}, t)\rho(\mathbf{x}, t)d\mathbf{x}. \tag{32}$$

If the system is homogeneous enough, Λ becomes a constant, positive or negative. Thus, since $N = \int_{\mathbf{x}} \rho d\mathbf{x}$, the population will grow or shrink exponentially until an equilibrium state is reached, when $\Lambda = 0$, i.e.,

$$N(t) = N_0 e^{\Lambda t}. \tag{33}$$

Phase Transitions

If we assume that the system is homogeneous and we introduce a perturbation along the x axis, from Eq. (7) it follows

$$\dot{P} = \left(\frac{\gamma}{2} - D_\theta\right)P, \tag{34}$$

where $P = \|\mathbf{P}_1\|$ is the polar order. Thus, $\gamma_p = 2D_\theta$ marks a transition from disorder to polar ordered systems. Moreover, solving Eq. (7) up to $n = 2$ and assuming $\gamma \gg D_\theta$ and $P > 0$, it follows

$$\dot{Q} = \left(\gamma - \frac{v_0}{2}\right)P, \tag{35}$$

where $Q = \|\mathbf{P}_2\|$ is the nematic order. Thus, $\gamma_n = v_0/2$ marks a transition to nematic ordered systems. (Fig. 2).

Absorbing Phases

Let's consider a single patch populated by n agents. The energetic equilibrium is given by

$$\begin{aligned} f_{eq}(n) &= c\left[1 - \frac{I_s}{r}n\right], \\ e_{eq}(n) &= \frac{I_s}{m}c\left[1 - \frac{I_s}{r}n\right] - \frac{k}{m}v_0^2. \end{aligned} \tag{36}$$

These energies are maximums for $n = 0$ (an unpopulated patch) and decrease linearly with n until vanish. The reproduction and the starvation numbers are defined as

$$\begin{aligned} n_r &= \frac{r}{I_s}\left[1 - \frac{me_r + kv_0^2}{cI_s}\right], \\ n_s &= \frac{r}{I_s}\left[1 - \frac{me_s + kv_0^2}{cI_s}\right], \end{aligned} \tag{37}$$

by taking $e_{eq} = e_r$ and $e_{eq} = e_s$ respectively. In patches where $n \leq n_r$ agents will reproduce, while in patches with $n \geq n_s$ agents will die. Therefore, the equilibrium population in a single patch n_{eq} satisfy

$$n_r < n_{eq} < n_s. \tag{38}$$

In the limit $v \to 0$, there is no exchange of agents between patches, so the population in each patch is constant. If, in such conditions, $n_s \leq 1$, the patches are unable to support life and the agents become extinct. On the opposite limit, $v \to \infty$, the exchange of agents between patches happens so fast that we can consider that each patch contains, on average, $\bar{n} = N/M$ agents. In this regime, the total population satisfies

$$n_r M < N_{eq} < n_s M. \tag{39}$$

Thus, in systems where $0 < n_s \leq 1$ will occur a phase transition. The mean squared displacement of an agent, in the case of a persistent random walk, results

$$\left\langle [x(t) - x(0)]^2 \right\rangle = 4Dt. \tag{40}$$

Each agent reaches energetic equilibrium in a characteristic time $t_a = 1/m$. In that time, the agent must have visited a total of $1/n_s$ patches to ensure its survival. Considering that the number of patches visited by an agent in a time t is $\left\langle \Delta x^2 \right\rangle / L_p^2$, and that $v_0^2 \ll 1$, it follows

$$v_{0,min} = L_p I_s \sqrt{\frac{cmD_\theta}{2r}\frac{1}{cI_s - me_s}} \tag{41}$$

If the velocity is less than $v_{0,min}$, the population will fall to zero. If the velocity is greater than $v_{0,min}$, there will be a population given by Eq. (39). On the other hand, from Eq. (36) it follows that the maximum velocity for a population of agents is

$$v_{0,max} = \sqrt{\frac{cI_s - me_s}{k}}. \tag{42}$$

Any velocity above this limit leads to $n_s < 0$ and therefore to the agents extinction. Thus, the range of velocities that allow populations to flourish is limited both below and above. These absorbing phases are clearly shown in Fig. 2.

Dynamical Features and Energetics

Beyond the steady-state phases, the system exhibits rich temporal dynamics and energetic constraints. Fig. 4(a,b) illustrates the time evolution of the emergent order. Starting from a disordered state ($O \approx 0, S \approx 1$), the system undergoes a two-stage relaxation process: first, a rapid equilibration of internal energies ($t \approx 10^2$), followed by a slower symmetry-breaking transition ($t \approx 4 \cdot 10^3$) where collective behavior emerges and the order parameters saturate to their γ-dependent steady values.

The population dynamics are governed by stability thresholds derived from the energy landscape. As shown in Fig. 4(c,d), the steady-state population density $\langle n_{\rm eq} \rangle$ is an attractor within the viability range $[n_r, n_s]$. However, the basin of attraction is bounded: initial populations exceeding a critical density $\langle n_c(0) \rangle \approx 2.6$ trigger a catastrophic collapse (extinction) due to rapid resource depletion before replenishment can occur.

Fig. 4(e) shows wave velocity β_m as a function of the angular noise τ, fitting Eqs. (12) and (14). Fig. 4(f) shows a histogram of the spatial distribution of velocities in a system with high nematic order, before, during, and after the collision between two opposing waves.

The metabolic efficiency of the system can be quantified by the total resource consumption rate $\Omega = \langle N \rangle (c\langle e \rangle + \kappa v_0^2)$. Figure 5 reveals that the mean field predictions for patch and agent energies hold well for dense populations ($n > 1$). Crucially, the system exhibits a consumption-maximizing density at $n \approx 1$, suggesting an optimal foraging strategy that balances population size with per-capita energy availability. This peak implies that intermediate population densities are most effective at exploiting the environmental energy flux.

[1] G. Briozzo, G. J. Sibona, and F. Peruani, Resource and population dynamics in an agent-environment interaction model, arXiv preprint arXiv:2512.08762 (Submitted to Phys. Rev. E) (2025).

[2] T. Vicsek and A. Zafeiris, Collective motion, Physics reports **517**, 71 (2012).

[3] M. C. Marchetti, J.-F. Joanny, S. Ramaswamy, T. B. Liverpool, J. Prost, M. Rao, and R. A. Simha, Hydrodynamics of soft active matter, Reviews of Modern Physics **85**, 1143 (2013).

[4] A. Cavagna, A. Cimarelli, I. Giardina, G. Parisi, R. Santagati, F. Stefanini, and M. Viale, Scale-free correlations in starling flocks, Proceedings of the National Academy of Sciences **107**, 11865 (2010).

[5] T. Vicsek, A. Czirók, E. Ben-Jacob, I. Cohen, and O. Shochet, Novel type of phase transition in a system of self-driven particles, Physical review letters **75**, 1226 (1995).

[6] M. E. Cates and J. Tailleur, Motility-induced phase separation, Annual Review of Condensed Matter Physics **6**, 219 (2015).

[7] P. Turchin and G. O. Batzli, Availability of food and the population dynamics of arvicoline rodents, Ecology **82**, 1521 (2001).

[8] A. J. Mathijssen, F. Guzmán-Lastra, A. Kaiser, and H. Löwen, Nutrient transport driven by microbial active carpets, Physical Review Letters **121**, 248101 (2018).

[9] R. Nathan, W. M. Getz, E. Revilla, M. Holyoak, R. Kadmon, D. Saltz, and P. E. Smouse, A movement ecology paradigm for unifying organismal movement research, Proceedings of the National Academy of Sciences **105**, 19052 (2008).

[10] J. M. Fryxell, M. Hazell, L. Börger, B. D. Dalziel, D. T. Haydon, J. M. Morales, T. McIntosh, and R. C. Rosatte, Multiple movement modes by large herbivores at multiple spatiotemporal scales, Proceedings of the National academy of Sciences **105**, 19114 (2008).

[11] E. F. Keller and L. A. Segel, Initiation of slime mold aggregation viewed as an instability, Journal of Theoretical Biology **26**, 399 (1970).

[12] B. Liebchen and H. Löwen, Synthetic chemotaxis and collective behavior in active matter, Accounts of chemical research **51**, 2982 (2018).

[13] G. Sibona, Evolution of microorganism locomotion induced by starvation, Physical Review E **76**, 011919 (2007).

[14] P. Forgács, A. Libál, C. Reichhardt, N. Hengartner, and C. Reichhardt, Using active matter to introduce spatial heterogeneity to the susceptible infected recovered model of epidemic spreading, Scientific Reports **12**, 11229 (2022).

[15] W. Ebeling, F. Schweitzer, and B. Tilch, Active brownian particles with energy depots modeling animal mobility, BioSystems **49**, 17 (1999).

[16] C. Condat and G. Sibona, Noise-enhanced mechanical efficiency in microorganism transport, Physica A: Statistical Mechanics and its Applications **316**, 203 (2002).

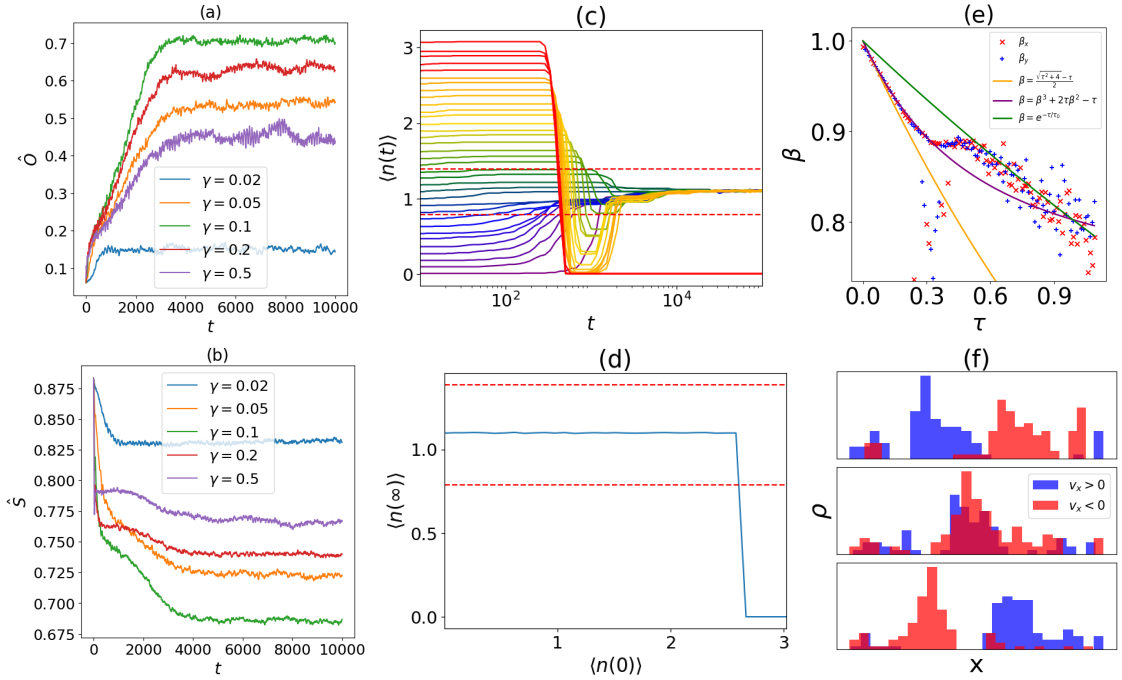

FIG. 4. **Temporal dynamics and stability.** (**a-b**) Time evolution of the mean nematic order $\hat{O}$ and spatial entropy $\hat{S}$ from a disordered initial state ($N_i = 200, v_0 = 2^{-0.5}$). The system relaxes to a steady state determined by γ after a transient period. (**c**) Evolution of population density $\langle n(t) \rangle$ for various initial densities $\langle n(0) \rangle$. Red dashed lines indicate reproduction (n_r) and starvation (n_s) thresholds. Populations starting within or below the stable range converge to an equilibrium $\langle n_{\text{eq}} \rangle \approx (n_r + n_s)/2$. Those starting above n_s exhibit damped oscillations, while excessive initial densities ($\langle n(0) \rangle > n_c \approx 2.6$) lead to extinction. (**d**) Equilibrium population as a function of initial density, confirming the extinction threshold. (**e**) Center-of-mass velocity components vs. noise parameter τ for $\gamma = 0.10$. Below the critical threshold $\tau < \tau_c$, wave motion is stable and unidirectional (one component dominates). Near τ_c, fluctuations destabilize the direction, and for $\tau > \tau_c$, coherent motion vanishes. (**f**) *Ripple effect* mechanism ($\gamma = 0.5, D_\theta = 0.0015$): Spatial histograms of agent density before, during, and after a collision event, showing the interpenetration of counter-propagating clusters (red: right-moving, blue: left-moving).

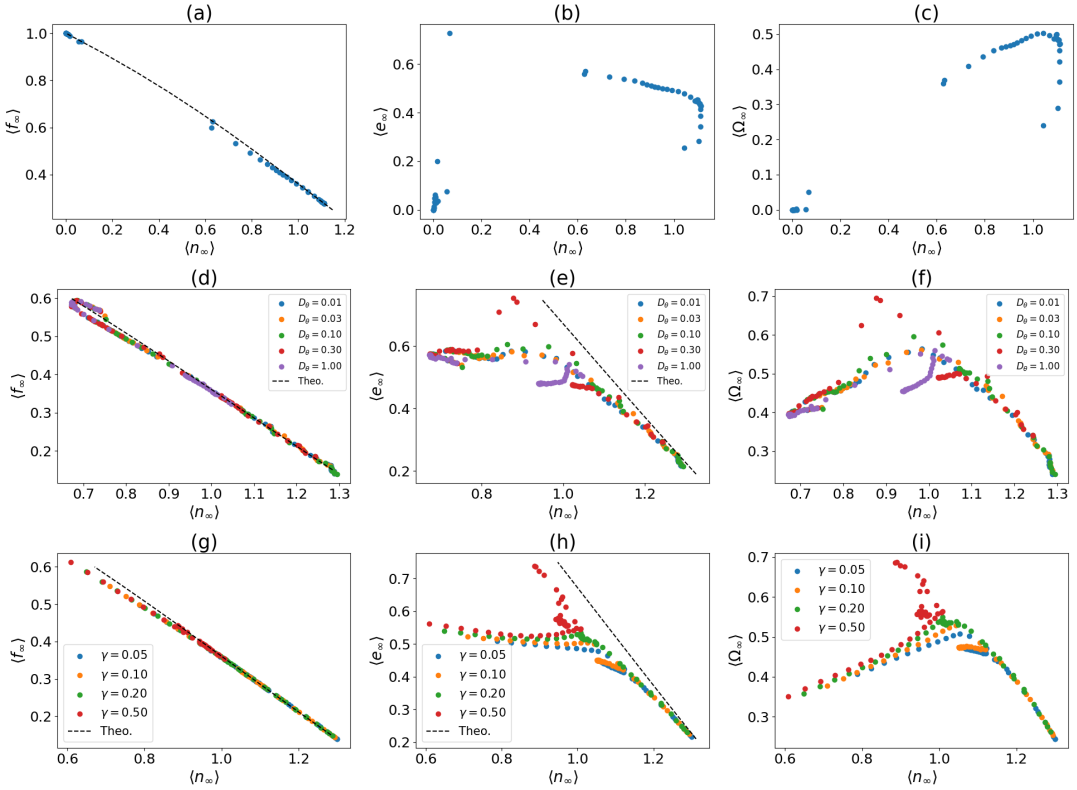

FIG. 5. **System energetics and consumption.** Steady-state averages of patch energy $\langle f \rangle$ (1st col), agent energy $\langle e \rangle$ (2nd col), and total consumption rate Ω (3rd col) plotted against the implicit equilibrium population $\langle n_\infty \rangle$. Rows correspond to variations in active velocity v_0 (top), alignment force γ (middle), and angular diffusion D_θ (bottom). The data reveals that: (i) Patch energies (left column) follow the mean-field prediction (dashed lines) robustly. (ii) Agent energies (center column) deviate from mean-field theory at high energies/low populations due to fluctuations. (iii) The total consumption Ω (right column) exhibits a distinct maximum near $\langle n_\infty \rangle \approx 1$, identifying an optimal density for resource exploitation efficiency.